Energy & Environmental Science

PAPER

View Article Online
View Journal | View Issue

Cite this: *Energy Environ. Sci.*, 2014, **7**, 1489

Efficient CO_2 capture by humidified polymer electrolyte membranes with tunable water state†

Yifan Li,[ab] Qingping Xin,[ab] Hong Wu,[ab] Ruili Guo,[c] Zhizhang Tian,[ab] Ye Liu,[ab] Shaofei Wang,[ab] Guangwei He,[ab] Fusheng Pan[ab] and Zhongyi Jiang*[abc]

Received 20th September 2013
Accepted 23rd January 2014

DOI: 10.1039/c3ee43163k

www.rsc.org/ees

Polymer electrolyte membranes containing alkali or alkaline-earth metal salts were designed and utilized for CO_2 capture. These membranes showed higher CO_2 permeability than the un-doped control membrane due to the increase of water content, and CO_2/gas selectivity was simultaneously enhanced due to the "salting-out" effect, which was strongly dependent on the content of bound water. More specifically, water content, water state and separation performance of polymer electrolyte membranes were strongly dependent on the salt type: (1) membranes containing alkaline-earth metal salts displayed a higher amount of bound water than those containing alkali cations, because the hydration energy of the alkaline-earth cation is relatively larger than that of the alkali cation; (2) the salts (KCl and $CaCl_2$) that can efficiently interrupt chain packing by metal–polymer complexation facilitated the diffusion of water molecules into the polymer matrix and thus increased the total amount of absorbed water. As a consequence, $CaCl_2$-doped membranes showed the highest CO_2 permeability (2030 Barrer) and a high separation factor (108 for CO_2/N_2 and 31 for CO_2/CH_4) at 2 bar (gage pressure) and 298 K for fully humidified gas streams. The effects of annealing conditions and feed pressure were also explored to elucidate the relevant separation mechanism of the polymer electrolyte membrane.

Broader context

Membrane technology possesses great potential in CO_2 capture, while membranes with high performance and low cost are still urgently required. Polymeric hydrogel membranes show high CO_2 permeability, but the presence of large amount of free water often leads to low CO_2/gas selectivity and poor operation stability. An appropriate water content and water state are crucial to achieve high CO_2 capture performance. In this study, a series of polymer electrolyte membranes were designed and prepared by incorporating alkali or alkaline-earth metal salts into the Pebax matrix. The effects of salt type and salt content on the water content, water state and CO_2 capture properties were investigated. Due to the well-controlled total water and bound water content within membrane, both CO_2 permeability and CO_2/gas selectivity were significantly elevated, surpassing the upper bound reported in 2008. It is notable that the CO_2 capture performance of polymer electrolyte membranes showed relatively weak dependence on feed pressure, compared to the amino-containing facilitated transport membranes. This finding may have useful implications in designing high-performance and cost-effective membranes for CO_2 capture. More polymer electrolyte membranes comprising different polymers and salts are expected to be explored.

1. Introduction

Global attention has been focused on efficient capture of CO_2 from a huge amount of energy-related industrial gases, such as natural gas, biogas, flue gas, *etc.*[1–3] The polymer-based membrane has shown great potential in CO_2 capture for the excellent processability and mass productivity, while the well-known "tradeoff" between permeability and selectivity has long restricted the performance of polymeric membranes.[4–7] Based on the solution-diffusion model, the overall selectivity originates from both solubility selectivity and diffusivity selectivity, and enhancing solubility selectivity has been known as one of the most popular and effective routes to astriding the "tradeoff" hurdle.[8,9] In particular, since CO_2 is much more condensable than other light gases, polar groups that can favorably interact with CO_2 are usually required to endow the membrane with high solubility selectivity. Unfortunately, the polar groups on flexible polymer chains often result in high polymer cohesion energy and a concomitant low free volume, which is unfavorable for the transport of fast gas.[10]

Many efforts have been devoted to solving the aforementioned sticky problem, and the relevant research can be

[a]*Key Laboratory for Green Chemical Technology of Ministry of Education, School of Chemical Engineering and Technology, Tianjin University, Tianjin 300072, China. E-mail: zhyjiang@tju.edu.cn; Fax: +86 22 23500086; Tel: +86 22 23500086*

[b]*Collaborative Innovation Center of Chemical Science and Engineering (Tianjin), Tianjin 300072, China*

[c]*Key Laboratory for Green Process of Chemical Engineering of Xinjiang Bingtuan, School of Chemistry and Chemical Engineering, Shihezi University, Shihezi 832003, Xinjiang, China*

† Electronic supplementary information (ESI) available. See DOI: 10.1039/c3ee43163k

summarized into two categories: (1) water-free CO_2 capture membranes (*e.g.* polyimides of high free volume,[11,12] thermally rearranged polymers[13–15] and polymers of intrinsic microporosity[10,16–18]), of which the large free volume cavities/pores arise from the inefficient packing of their extremely rigid blocks, but suffer from blockage when water is present; (2) water-facilitated CO_2 capture membranes (*e.g.* facilitated transport membrane[19–24]), and the high free volume of these membrane materials arises from water-induced swelling. In recent years, gas transport through different kinds of polymeric membranes with the mediation of water has gained growing interest.[4,25–32] Polymeric membrane materials with flexible main chain and hydrophilic side chain were usually selected to take the advantage of swelling and to avoid the blockage of gas transport route arising from the dominating water adsorption. However, the large extent of membrane swelling due to the high hydrophilicity restricts the overall selectivity. For example, CO_2/N_2 selectivity of water-swollen hydrogel membranes containing a very high amount of water is somewhat like that in bulk water (only about 50 at 25 °C), which is far from economical CO_2 capture.[23,33] Furthermore, the excessive amount of water is mainly free water, which contributes little to CO_2 permeability but brings about new problems such as instability.[33] Exploring new polymer-based membranes with high CO_2/gas selectivity under low water content is thus highly desirable.

The polymer electrolyte membrane comprising the hydrophilic polymer and salt has been widely employed for fast ion conduction,[34,35] while this concept has rarely been utilized in membrane gas separation. Very recently, the water molecules organized around metal ions have been reported to have significantly lowered solubility of non-polar gases and therefore exhibit a salting-out effect.[27] Furthermore, the hydrated and ionized form of CO_2 (*e.g.* HCO_3^-) is expected to transport through the polymer electrolyte membrane much faster than non-ionized gases. Another benefit of the polymer electrolyte membrane is the tunable complexation interactions between polymer chains and metal ions, which is envisaged to control membrane swelling without sacrificing membrane hydrophilicity. Thirdly, salt as doping additive is not volatile as the commonly utilized amino-bearing molecules, which is profitable to membrane stability. Consequently, it can be expected that the design of polymer electrolyte membrane with tunable water content and water state might be a promising approach to achieve efficient and economical CO_2 capture.

Herein, a series of polymer electrolyte membranes were fabricated by doping alkali or alkaline-earth metal salts into Pebax, a polyethylene oxide (PEO)-based copolymer with high solubility selectivity and abundant availability.[36,37] CO_2 capture properties of the membranes were tested under both dry state and humidified state. The effect of salt type and salt content on the water state and CO_2 capture properties of the membrane were investigated, and the relationship between water state and CO_2 capture properties was depicted. To further elucidate the separation mechanism of the polymer electrolyte membrane, the effects of annealing conditions and feed pressure were also examined.

2. Experimental

2.1 Materials

Pebax(R) MH 1657 (the chemical structure is shown in Scheme 1) was purchased from Arkema (Paris, France). $LiCl\cdot H_2O$, NaCl, KCl, $MgCl_2\cdot 6H_2O$ and $CaCl_2$ were purchased from Tianjin Guangfu Fine Chemical Research Institute (Tianjin, China), including ethanol. All chemicals were of reagent grade or higher, and were used without further purification.

2.2 Membrane preparation

Pebax was dissolved in ethanol–water (70/30 wt%) under mild mechanical stirring (with reflux) at 80 °C for 3 h to obtain 5 wt% homogeneous solution. After cooling the solution to ambient temperature, a certain amount of metal chloride salt powder, such as $LiCl\cdot H_2O$, NaCl, KCl, $MgCl_2\cdot 6H_2O$ and $CaCl_2$, was dissolved into the solution followed by 2 h stirring. The molar ratio of salt to ethylene oxide (EO) unit was controlled at 0, 1 : 60, 1 : 30, 1 : 15 and 1 : 7.5, respectively. After removing bubbles, the homogeneous solutions were cast onto Teflon Petri dishes and then dried under ambient conditions for 24 h. The membranes were further annealed in a vacuum oven at 45 °C for three days to remove the residual solvent. The resultant membranes were designated as Pebax, where salt was absent, or Pebax–Y(*X*), where *X* means the molar ratio of salt to ethylene oxide unit, and Y represents the type of salt, which can be LiCl, NaCl, KCl, $MgCl_2$, or $CaCl_2$. The thickness of all membranes was controlled within the range of 80–90 μm.

2.3 Gas permeation experiments

Single CO_2, CH_4, N_2 and binary CO_2–CH_4 (30 vol% : 70 vol%), CO_2–N_2 (10 vol% : 90 vol%) gas permeation experiments were conducted at 25 °C based on the conventional constant pressure/variable volume technique (the scheme of apparatus is shown in Fig. S1†). N_2 was selected as sweep gas when no N_2 existed in feed gas, while CH_4 was utilized as a sweep gas to determine the permeability of N_2. In a typical measurement, 2 bar of feed gas (gage pressure) was firstly introduced into a water bottle (35 °C) to be saturated with water vapor, and then passed through an empty bottle to remove the residual water. Meanwhile, the sweep gas was humidified at room temperature. The flow rate and composition of sweep gas were recorded every 5 minutes until they no longer varied with time. For comparison, dry-state gas permeation experiments were also conducted, in which case the feed gas and sweep gas were directly introduced into the membrane cell.

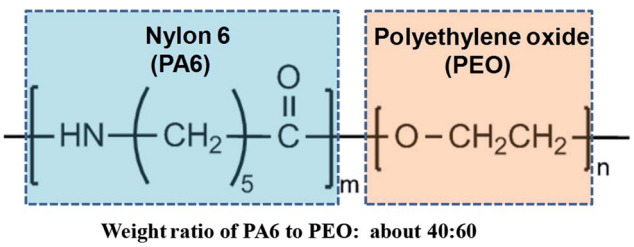

Scheme 1 Chemical structure of Pebax 1657.

The compositions of the feed, retentate, and permeate were measured using gas chromatography. The permeability (P_i, Barrer, 1 Barrer = 10^{-10} cm^3 (STP) cm^{-2} s^{-1} cm^{-1} Hg) of either gas was obtained from the average value of at least 2 tests by eqn (1):

$$P_i = \frac{Q_i l}{\Delta p_i A} \quad (1)$$

where Q_i is the volumetric flow rate of gas 'i' (cm^3 s^{-1}) at standard temperature and pressure (STP), l is the membrane thickness (cm), Δp_i is the transmembrane partial pressure difference of gas 'i' (cm Hg), and A is the effective membrane area (12.56 cm^2). The ideal selectivity (α_{ij}) was calculated by eqn (2):

$$\alpha_{ij} = \frac{P_i}{P_j} \quad (2)$$

Since the permeate side is maintained at ambient pressure, the mixed-gas separation factor could be also calculated by eqn (2).

2.4 Measurement of total water, free water and bound water

Water uptake and water state were determined following the reported procedure.[21] Each membrane was weighed to determine the "humidified" weight (m_1, mg) after gas permeation, and then heated at 100 °C in a vacuum oven for 6 h to remove free water. The membranes were reweighed (m_2, mg) and further dried under vacuum at 150 °C for another 6 h. The completely dried membranes were weighed again to determine their "dried" weight (m_0, mg). In this way, the content of total water (W_t, %), free water (W_f, %) and bound water (W_b, %) were calculated based on the following equations:

$$W_t = (m_1 - m_0)/m_0 \times 100\% \quad (3)$$

$$W_f = (m_1 - m_2)/m_0 \times 100\% \quad (4)$$

$$W_b = (m_2 - m_0)/m_0 \times 100\% \quad (5)$$

It should be mentioned that the adsorbed CO_2 within membrane had little effect on determination of water uptake and water state. The permeation test of Pebax–$CaCl_2$ (1 : 30) was performed more than twice to quantify the amount of CO_2 when the feed gas is removed. The membrane after test was immersed into 1 mM fresh aqueous ammonia for 15 min and then the remaining amount of ammonia was measured by the acid–base titration method. The amount of CO_2 within the membrane was therefore calculated as 0.21 ± 0.02 wt%, which was significantly lower than water uptake (>5 wt%) and free water (>4.5 wt%). Despite the relatively smaller difference between CO_2 uptake and bound water content (<2 wt%), the absorbed CO_2 could completely release when measuring the amount of free water.

2.5 Measurement and prediction of membrane density

Experimental values of membrane density were determined at 25 °C by the buoyancy method using an electronic balance (OHAUS®, CP224C) equipped with a density determination kit. Silicon oil with known density (ρ_0 = 0.972 g cm^{-3}) was selected as the auxiliary liquid. Experimental values of density (ρ_B) were calculated by the following eqn (6):

$$\rho_B = \frac{M_A}{M_A - M_L}\rho_0 \quad (6)$$

where M_A and M_L are the membrane weight in the air and in the liquid, respectively.

Membrane density was also predicted by the additive model. Since the most stable forms of salts at ambient temperature (after annealing at 45 °C) are $LiCl \cdot H_2O$, NaCl, KCl, $MgCl_2 \cdot 6H_2O$ and $CaCl_2 \cdot 2H_2O$, their density data were employed to estimate membrane density. Notably, the density of the humidified membrane was predicted by assuming that salt was completely or partially dissolved by the adsorbed water (mentioned in Section 2.4), depending on the solubility and content of salt. If salt was completely dissolved, membrane density was calculated by assuming unsaturated salt solution as the additive. If salt was partially dissolved, the membrane density was calculated by assuming saturated salt solution and the residual salt crystal as the two additives. The density of salt solution was obtained by measuring the weight and volume of a certain amount of salt solution, of which the salt concentration was determined on the basis of the assumed salt solution within membrane. In this way, the calculated density of the humidified membrane could be calibrated by considering the effect of binary interactions between salt and water.

2.6 Calculation of fractional free volume (FFV)

FFV was calculated based on the density data. The FFV of pure Pebax (defined as FFV_P) was estimated by eqn (7):

$$FFV_P = 1 - 1.3\nu_w\rho_P \quad (7)$$

where ρ_P is the density of Pebax, and ν_w is the van der Waal's volume of the repeat unit of Pebax in cm^3 g^{-1}, which was calculated as 0.590 cm^3 g^{-1} using the group contribution method[38] considering only the amide –[CO–$(CH_2)_5$–NH]– and ether –[$(CH_2)_2$O]– segments in the structure of Pebax-1657 shown in Scheme 1. The FFV values of dry state polymer electrolyte membranes were calculated by simultaneously solving eqn (8)–(11) following Yave's method:[39]

$$\phi_S = \frac{w_S/\rho_S}{w_P/\rho_P + w_S/\rho_S + v_V} = w_S\frac{\rho_B}{\rho_S} \quad (8)$$

$$\phi_P = \frac{w_P/\rho_P}{w_P/\rho_P + w_S/\rho_S + v_V} \quad (9)$$

$$\phi_V = \frac{v_V}{w_P/\rho_P + w_S/\rho_S + v_V} \quad (10)$$

$$FFV = FFV_P\phi_P + \phi_V \quad (11)$$

where ϕ_S, ϕ_P and ϕ_V are the true volume fractions of salt, polymer and void volume, respectively, w_S, w_P, ρ_S, and ρ_P are the weight percents and densities of salt and pure polymer,

respectively, and v_V was the void volume. To estimate the FFV of humidified membranes, each membrane was perceived as a combination of four components: salt solution, salt (depending on whether the salt solution was saturated), polymer, and void volume, and the volume fraction of salt solution was also considered as FFV.

2.7 Membrane characterization

The distribution of salts in membranes were investigated using a Nanosem 430 field emission scanning electron microscope (FESEM), equipped with energy dispersive X-ray (EDX) spectroscopy (see Fig. S2†). Thermal properties of samples were measured under nitrogen atmosphere by Differential Scanning Calorimetry (DSC) module (DSC 200F3, NETZSCH), with the temperature rising from −70 to 250 °C at a heating rate of 10 °C min^{-1}. The chemical structure of membrane was characterized by a Nicolet-560 Fourier transform infrared spectrometer (FT-IR) with a scan range of 4000–400 cm^{-1}. The crystalline structures of membranes were determined using wide-angle X-ray diffraction (WAXD) in the range of 10–50° at the speed of 10° min^{-1} (Rigaku D/max 2500 v/pc, CuK 40 kV, 200 mA, λ = 1.5406 Å). The Young's modulus, break strength and maximum elongation of a sample were determined by a material testing machine (AXM350-10KN, Testometric Co., Germany) with the extension rate of 7 mm min^{-1}.

3. Results and discussion

3.1 Gas transport properties

Pure-gas permeation tests were performed to probe the intrinsic gas transport properties of membrane materials. As shown in Fig. 1, all salt-doped polymer electrolyte membranes exhibit superior performance to the salt-free pristine membrane under the humidified state, and the membranes doped with alkaline-earth metal salt outperform those doped with alkali metal salt. For example, the membranes doped with $CaCl_2$ display the highest CO_2 permeability and high CO_2/CH_4 and CO_2/N_2 selectivity, while $MgCl_2$-doped membranes display the highest selectivity and moderate permeability. Fig. 1 also shows that CO_2 permeability, CO_2/CH_4 selectivity and CO_2/N_2 selectivity firstly increase simultaneously with the increment of salt content, and then do not evidently vary with salt content until the molar ratio of salt to EO is higher than 1 : 30. Especially, ideal CO_2/CH_4 selectivity above 35 and CO_2/N_2 selectivity above 140 are achieved for Pebax–$CaCl_2$ (1 : 30) and Pebax–$MgCl_2$ (1 : 30), which are significantly higher than those of pristine Pebax. As shown in Fig. 2, most of the performance data of humidified membranes surpass the updated upper bound reported in 2008,[7] while those of the dry membrane fall far below that line. From another viewpoint, both permeability and selectivity are significantly enhanced after humidification for

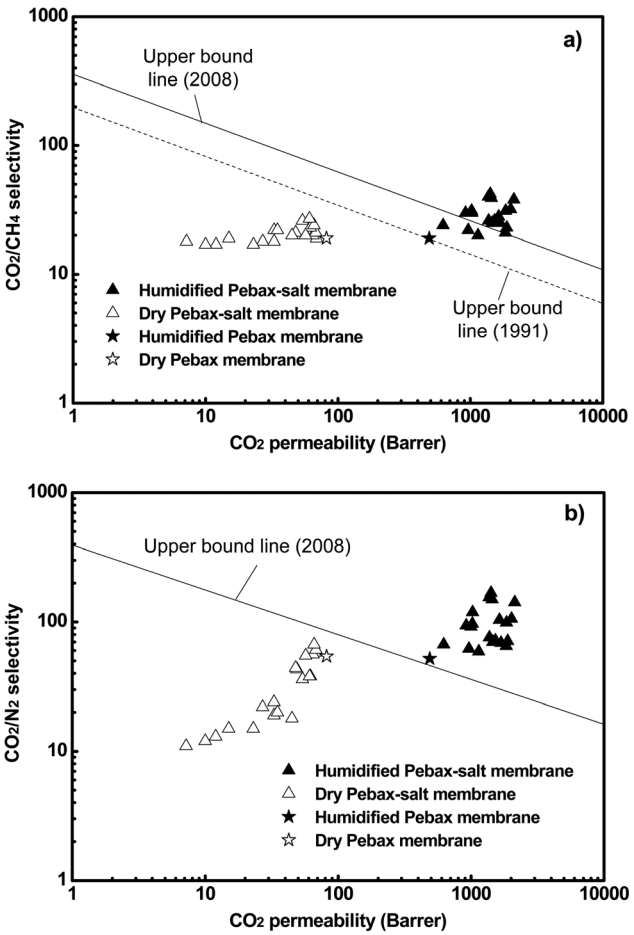

Fig. 2 Gas separation performance of the membranes in this study (feed gas: pure gases; temperature: 25 °C; pressure: 2 bar).

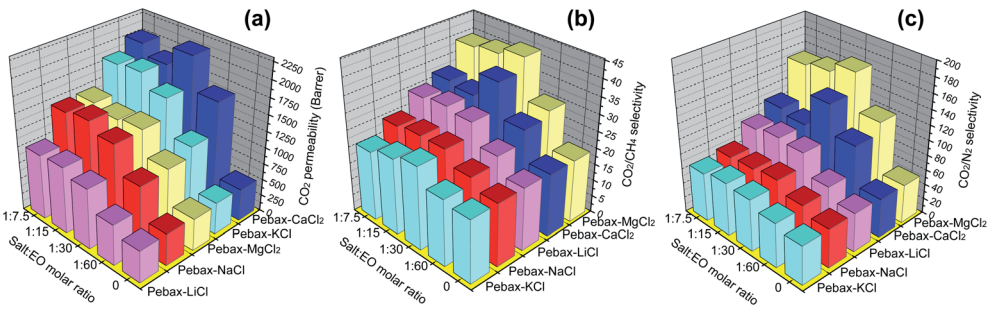

Fig. 1 Effect of salt type and content on (a) CO_2 permeability (b) CO_2/CH_4 selectivity and (c) CO_2/N_2 selectivity (feed gas: pure gases; temperature: 25 °C; pressure: 2 bar).

salt-doped polymer electrolyte membranes, while humidification does not improve the selectivity of Pebax. It is inferred that both salt and water contribute to such encouraging results, which will be thoroughly discussed below. The effect of salt content on the membrane structure and performance will be also elucidated in the following statement.

3.2 Structure–property relationships

The total water, free water and bound water of all membranes were analysed to pursue rational explanation of the selectivity mechanisms of polymer electrolyte membranes. As shown in Fig. 3, the membranes doped with alkaline-earth metal salt contains higher amount of water (especially bound water) than other membranes. Fig. 4 and 5 clearly reveal the relationship between the water uptake and CO_2-selective permeation: high W_t corresponds to high CO_2 permeability, and high W_b corresponds to high CO_2/gas selectivity. It can be easily understood that high W_t plasticizes the polymer chains and leads to high CO_2 permeability. The close relationship between selectivity and bound water can be interpreted by the "salting-out" hypothesis: the bound water molecules surrounding metal ions lose the capacity of dissolving non-condensable gases to a large extent, and then disrupt the continuity of their transport routes. In addition, the water binding with the EO and amide groups of Pebax may facilitate the hydration of CO_2 and the generation of HCO_3^-, which is able to permeate through the electrolyte membrane with much lower energy barrier. As such, high bound water results in relatively lower transport resistance of CO_2 than those of CH_4 and N_2, and hence highly CO_2-selective membrane.

The amount of absorbed water and water state in the salt-doped membrane largely depend on salt type, in particular, the metal ion type. As seen from Fig. 2, the sequence of membrane bound water at the same salt loading is: Pebax–$MgCl_2$ > Pebax–$CaCl_2$ > Pebax–LiCl > Pebax–NaCl > Pebax–KCl, which is in good accordance with the sequence of hydration free energy for the five metal ions: Mg^{2+} (1907 kJ mol^{-1}) > Ca^{2+} (1594 kJ mol^{-1}) > Li^+ (511 kJ mol^{-1}) > Na^+ (411 kJ mol^{-1}) > K^+ (337 kJ mol^{-1}).[40] This suggests that the high hydration tendency of the metal ion can be transferred to the corresponding polymer electrolyte membrane, and further affect membrane selectivity. Whereas, the sequence of membrane total water at the same salt loading is: Pebax–$CaCl_2$ > Pebax–KCl > Pebax–$MgCl_2$ > Pebax–NaCl > Pebax–LiCl, which is different from the sequence of hydration free energy discussed above. It is hypothesized that the fourth-period metal ions (Ca^{2+} and K^+) form more stable complexation with PEO and PA6, and hence break the hydrogen bond among the polar groups in a more efficient way. As such, water can be absorbed into the membrane at lower diffusion resistance. For the metal ions in the same period of periodic table of the elements, the difference in the ion size is too slight, in which case the net charge of metal ion plays the dominate role. The complexation ability of multivalent metal ions was reported to be higher than that of univalent ones.[41]

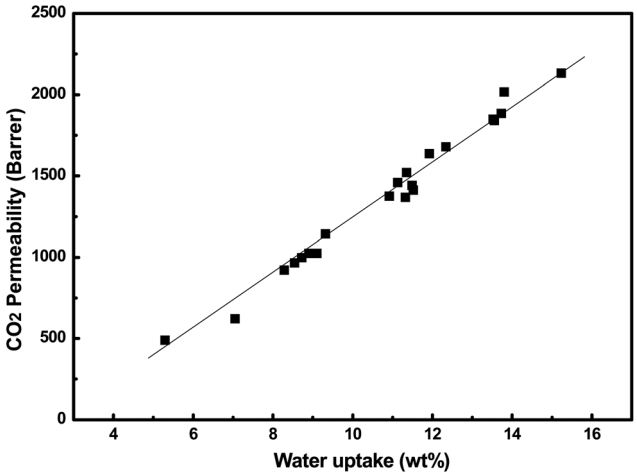

Fig. 4 Correlations between pure-gas CO_2 permeability and water uptake of the membrane.

Since $CaCl_2$-doped membranes display the highest CO_2 permeability and high CO_2/CH_4 and CO_2/N_2 selectivity, herein $CaCl_2$-doped membranes are chosen as representative samples to elucidate the effect of salt content. As shown in Fig. 3, Pebax–$CaCl_2$ (1 : 30) exhibits the highest total water, free water and bound water, and therefore the best performance. The less pronounced effect of excessively doped $CaCl_2$ at high content can be interpreted based on the following facts: (1) crystalline peaks of $CaCl_2$ appear for Pebax–$CaCl_2$ (1 : 15) and Pebax–$CaCl_2$ (1 : 7.5) (see WAXD data in Fig. S3†), which demonstrates that $CaCl_2$ has stronger tendency to self-crystallization than complex with polymer chains under such high loadings, that is, Pebax has been saturated with $CaCl_2$; (2) the crystalline degree of PEO

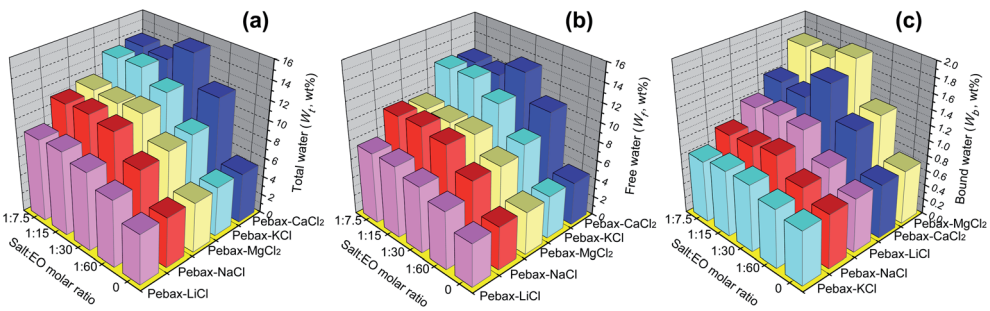

Fig. 3 The content of (a) total water (W_t) (b) free water (W_f) and (c) bound water (W_b) of the humidified membranes.

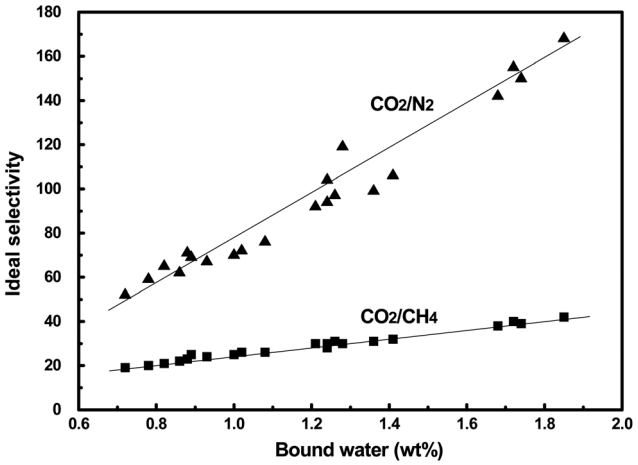

Fig. 5 Correlations between pure-gas CO_2/CH_4, CO_2/N_2 selectivity and bound water content of the membrane.

segment decreases significantly and the melting peak of PA6 diminishes under high $CaCl_2$ loading (see Table 1), suggesting that the majority of PEO and PA6 segments are complexed with Ca^{2+} at high $CaCl_2$ content, and the "ion-crosslinked" membranes become less gas-permeable (see the CO_2 permeability of dry membranes in Table 2); (3) FT-IR spectra (Fig. S4†) and Young's Modulus (Table S1†) also demonstrates that PEO–Ca^{2+} and PA6–Ca^{2+} interactions become apparently stronger at high $CaCl_2$ content, which further supports the phenomenon of ion-induced interchain crosslinking.

In order to clarify the effect of ionic crosslinking on separation mechanisms, herein the structure and performance of dry membranes and humidified membranes are thoroughly compared. (1) Table 1 demonstrates that at dry state the glassy transition temperatures (T_gs) of salt-doped membranes are higher than the salt-free membrane, which is in good accordance with the occurrence of ionic crosslinking. However, each membrane exhibit similar T_g to each other under the humidified state, which is almost independent of the salt type. It appears that water can significantly affect the chain rigidity of Pebax, and therefore the probable chain rigidification caused by ionic crosslinking does not happen for humidified membranes. (2) The effects of salt and water on chain rigidity are also supported by density measurement. By comparing the predicted and experimental density data, the variation of FFV can be roughly estimated. As shown in Table 3, for all humidified membranes the experimental density is lower than the predicted value, confirming that the remaining water within membrane lead to higher chain flexibility and FFV. In particular, $CaCl_2$-doped polymer electrolyte membranes display higher FFV than other types of membranes, which agrees well with the permeability data. In contrast, for all the dry membranes containing salts, the experimental density is higher than the predicted value, demonstrating that it is only under the dry state that the effect of ionic crosslinking will become apparent. (3) By comparing the gas transport properties under dry state and humidified state (Table 2), the effects of ionic crosslinking and water can be also separately concluded. For dry membranes, the addition of salt lead to higher selectivity and lower permeability at low salt content, reflecting the well-known "tradeoff" effect. However, dry-state polymer electrolyte membranes show lower CO_2/N_2 and CO_2/CH_4 selectivity than the control membrane at high salt content, especially for CO_2/N_2 selectivity. Actually, excessive ionic crosslinking will decrease the electron cloud density around the oxygen atoms of EO units, and therefore the dipole–quadrupole interactions between EO units and CO_2 are weakened. Since the separation of CO_2 from N_2 usually relies heavily on the difference in polarity rather than size,[17] the decrement of CO_2/N_2 selectivity with addition of salt is more obvious than that of CO_2/CH_4 selectivity. That is, at high salt loading, the preferential sorption is intensively interrupted for dry membranes (as supported by the "time-lag" experiment data in Table S2†), and both permeability and selectivity are declined. In sharp contrast, the humidified polymer electrolyte membranes with high salt content show both higher permeability and selectivity than the humidified control membrane, demonstrating that the "salting-out" effect represents the dominating selectivity mechanism in humidified polymer electrolyte membranes. The introduction of moisture weakens

Table 1 Thermal properties of Pebax and salt-doped polyelectrolyte membranes

	Dry membrane					Humidified membrane[a]		
	PEO segment			PA6 segment		PEO segment	PA6 segment	
Sample	T_g (°C)	T_m (°C)	X_c (%)	T_m (°C)	X_c (%)	T_g (°C)	T_m (°C)	X_c (%)
Pebax	−53.2	16.4	11.1	205.2	35.3	−56.0	205.0	35.8
Pebax–LiCl (1 : 30)	−51.3	17.6	11.5	201.5	33.6	−55.4	200.7	34.3
Pebax–NaCl (1 : 30)	−51.5	17.1	10.8	202.0	25.1	−55.8	201.5	27.1
Pebax–KCl (1 : 30)	−50.3	15.8	11.3	204.4	28.2	−55.6	204.0	31.1
Pebax–$MgCl_2$ (1 : 30)	−49.2	16.4	11.4	185.4	28.5	−55.5	184.8	30.5
Pebax–$CaCl_2$ (1 : 60)	−48.7	17.0	10.6	176.0	21.5	−55.2	175.4	27.6
Pebax–$CaCl_2$ (1 : 30)	−47.6	17.0	10.1	187.4	22.4	−55.0	186.6	25.7
Pebax–$CaCl_2$ (1 : 15)	−46.3	15.8	8.2	—[b]	—	−54.3	—	—
Pebax–$CaCl_2$ (1 : 7.5)	−44.2	11.6	0.6	—	—	−54.1	—	—

[a] The melting peak of the PEO segment was overlapped by that of bound water, and therefore T_m and X_c are not shown here. [b] "—" means no detectable melting peak.

Table 2 Comparison of pure-gas transport properties of the dry membranes and humidified membranes

	Dry membrane			Humidified membrane		
Sample	P_{CO_2}	α_{CO_2/CH_4}	α_{CO_2/N_2}	P_{CO_2}	α_{CO_2/CH_4}	α_{CO_2/N_2}
Pebax	82 ± 3.8	19 ± 0.3	54 ± 2.6	490 ± 28	19 ± 0.5	52 ± 2.0
Pebax–LiCl (1 : 60)	69 ± 1.9	19 ± 0.5	58 ± 4.0	622 ± 31	24 ± 1.6	67 ± 3.0
Pebax–LiCl (1 : 30)	49 ± 1.5	20 ± 0.4	43 ± 2.2	921 ± 29	30 ± 1.3	94 ± 5.2
Pebax–LiCl (1 : 15)	33 ± 0.3	22 ± 0.2	24 ± 1.1	1024 ± 25	31 ± 1.0	97 ± 4.0
Pebax–LiCl (1 : 7.5)	15 ± 0.4	19 ± 0.1	15 ± 0.8	998 ± 40	30 ± 1.3	92 ± 2.7
Pebax–NaCl (1 : 60)	65 ± 1.2	20 ± 0.4	56 ± 1.5	966 ± 33	22 ± 1.2	62 ± 2.5
Pebax–NaCl (1 : 30)	48 ± 1.5	21 ± 0.2	44 ± 2.0	1375 ± 64	26 ± 1.8	76 ± 4.1
Pebax–NaCl (1 : 15)	27 ± 0.3	18 ± 0.2	22 ± 1.0	1521 ± 18	26 ± 1.5	72 ± 0.9
Pebax–NaCl (1 : 7.5)	12 ± 0.6	17 ± 0.1	13 ± 0.5	1460 ± 27	25 ± 1.9	70 ± 2.7
Pebax–KCl (1 : 60)	68 ± 3.3	21 ± 0.5	61 ± 3.2	1143 ± 26	20 ± 0.8	59 ± 4.2
Pebax–KCl (1 : 30)	62 ± 2.0	23 ± 0.2	38 ± 2.0	1680 ± 45	25 ± 1.7	69 ± 2.8
Pebax–KCl (1 : 15)	33 ± 2.1	18 ± 0.3	19 ± 1.4	1885 ± 81	23 ± 1.4	71 ± 3.9
Pebax–KCl (1 : 7.5)	10 ± 0.4	17 ± 0.3	12 ± 0.4	1842 ± 65	21 ± 1.5	65 ± 2.3
Pebax–$MgCl_2$ (1 : 60)	57 ± 2.8	20 ± 0.3	55 ± 1.5	1025 ± 18	30 ± 2.2	119 ± 6.5
Pebax–$MgCl_2$ (1 : 30)	54 ± 2.4	26 ± 0.4	36 ± 2.0	1412 ± 71	42 ± 2.0	168 ± 2.3
Pebax–$MgCl_2$ (1 : 15)	45 ± 2.3	20 ± 0.3	18 ± 1.1	1369 ± 39	40 ± 2.6	155 ± 4.7
Pebax–$MgCl_2$ (1 : 7.5)	23 ± 1.8	17 ± 0.2	15 ± 0.4	1442 ± 24	39 ± 2.1	150 ± 7.4
Pebax–$CaCl_2$ (1 : 60)	66 ± 3.1	24 ± 0.3	67 ± 1.7	1638 ± 37	28 ± 0.9	104 ± 5.8
Pebax–$CaCl_2$ (1 : 30)	61 ± 2.0	27 ± 0.2	38 ± 1.2	2133 ± 74	38 ± 1.3	142 ± 2.6
Pebax–$CaCl_2$ (1 : 15)	35 ± 1.8	22 ± 0.1	20 ± 0.8	1850 ± 32	31 ± 1.6	99 ± 3.7
Pebax–$CaCl_2$ (1 : 7.5)	7.2 ± 0.2	18 ± 0.2	11 ± 0.5	2018 ± 55	32 ± 1.2	106 ± 6.2

the complexation of metal ion and Pebax, owing to the preferential water–metal ion interactions and water–polymer interactions. In this way, the affinity of EO units towards CO_2 is recovered. Furthermore, the water molecules tightly attached to metal ions not only facilitate the transport of CO_2, but also salt out CH_4 and N_2. In brief, humidification of the polymer electrolyte membranes reverses the negative effect of metal ions under dry conditions, and makes great contributions to the technologically attractive CO_2 capture properties.

We also tried to add $CaCO_3$ directly into Pebax to see whether insoluble calcium salt could lead to promising separation results, which is also important to understand the structure–property relationship of salt-doped membranes. The as-prepared mixed matrix membrane shows similar CO_2 permeability and CO_2/gas selectivity as Pebax at the humidified state. As a matter of fact, the Pebax–$CaCO_3$ blend is not a polymer electrolyte because $CaCO_3$ cannot be dispersed at the molecular level. Although $CaCO_3$ can be partially dissolved by CO_2 and H_2O, the transport of Ca^{2+} and HCO_3^- through the non-ionic polymer matrix is difficult. The comparison between the Pebax–$CaCl_2$ membrane and Pebax–$CaCO_3$ membrane further demonstrates the advantage of polymer electrolyte membranes.

3.3 Mixed-gas separation performance

To better understand the separation mechanism of the humidified polymer electrolyte membrane, time-dependent mixed-gas CO_2 capture properties of Pebax and Pebax–$CaCl_2$ (1 : 30) are plotted in Fig. 6. The following findings are notable: (1) high separation performance is maintained for CO_2/CH_4 and

Table 3 Densities and FFV values of the dry membranes and humidified membranes determined by the buoyancy method and additive model[a] (unit of density: g cm^{-3})

	Dry membrane				Humidified membrane			
Sample	ρ_B	ρ_M	$\rho_B - \rho_M$	FFV	ρ_B	ρ_M[b]	$\rho_B - \rho_M$	FFV
Pebax	1.140 ± 0.005	1.140	0 ± 0.005	0.126 ± 0.007	1.108 ± 0.004	1.133 ± 0.005	−0.025 ± 0.005	0.194 ± 0.012
Pebax–LiCl (1 : 30)	1.162 ± 0.007	1.151	0.011 ± 0.007	0.117 ± 0.008	1.115 ± 0.007	1.142 ± 0.006	−0.027 ± 0.007	0.237 ± 0.014
Pebax–NaCl (1 : 30)	1.166 ± 0.003	1.154	0.012 ± 0.003	0.117 ± 0.005	1.113 ± 0.006	1.142 ± 0.005	−0.029 ± 0.006	0.255 ± 0.007
Pebax–KCl (1 : 30)	1.168 ± 0.004	1.156	0.012 ± 0.004	0.116 ± 0.006	1.112 ± 0.005	1.146 ± 0.004	−0.034 ± 0.005	0.271 ± 0.010
Pebax–$MgCl_2$ (1 : 30)	1.181 ± 0.009	1.167	0.014 ± 0.009	0.109 ± 0.003	1.126 ± 0.008	1.159 ± 0.006	−0.033 ± 0.008	0.257 ± 0.013
Pebax–$CaCl_2$ (1 : 60)	1.169 ± 0.005	1.154	0.015 ± 0.005	0.114 ± 0.006	1.110 ± 0.010	1.148 ± 0.009	−0.038 ± 0.009	0.282 ± 0.017
Pebax–$CaCl_2$ (1 : 30)	1.183 ± 0.003	1.168	0.015 ± 0.003	0.111 ± 0.008	1.117 ± 0.005	1.151 ± 0.007	−0.034 ± 0.006	0.306 ± 0.015
Pebax–$CaCl_2$ (1 : 15)	1.209 ± 0.008	1.193	0.016 ± 0.008	0.107 ± 0.004	1.145 ± 0.012	1.176 ± 0.011	−0.031 ± 0.012	0.284 ± 0.012
Pebax–$CaCl_2$ (1 : 7.5)	1.255 ± 0.006	1.239	0.016 ± 0.006	0.099 ± 0.003	1.193 ± 0.010	1.218 ± 0.012	−0.025 ± 0.011	0.272 ± 0.009

[a] ρ_B and ρ_M mean the densities obtained by the buoyancy method and additive model, respectively. [b] Error bar is added because the calculation involves the density of salt solution, which was measured experimentally.

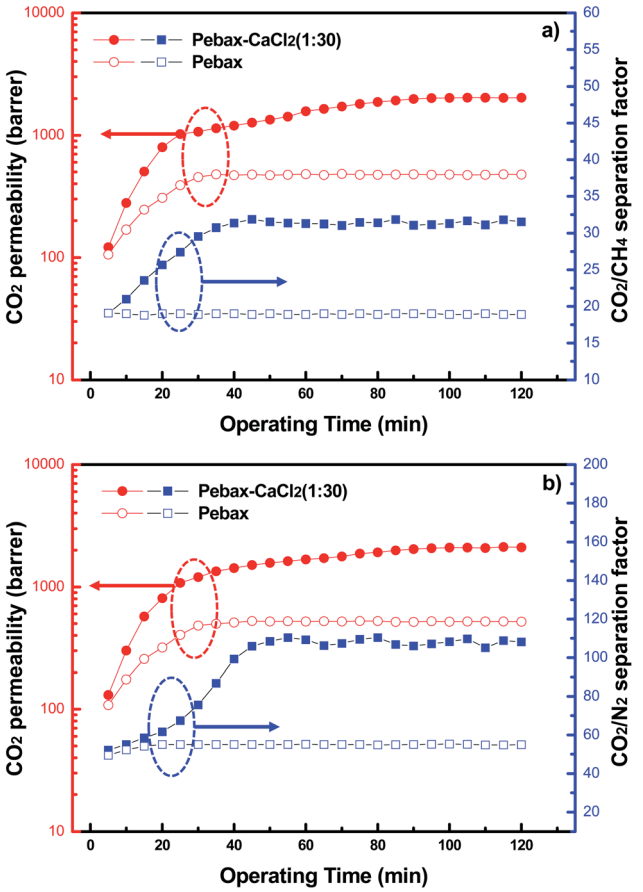

Fig. 6 Dynamic CO_2 capture properties of Pebax and Pebax–$CaCl_2$ (1 : 30): (a) CO_2/CH_4 separation; (b) CO_2/N_2 separation (feed gas: binary 30vol%CO_2–70vol%CH_4 gas and 10vol%CO_2–90vol%N_2, both are saturated with water vapor; temperature: 25 °C; pressure: 2 bar).

CO_2/N_2 separation, indicative of the CO_2-philic nature of Pebax–$CaCl_2$ (1 : 30); (2) during the first several minutes Pebax–$CaCl_2$ (1 : 30) does not take priority over Pebax, implying that it requires the balance of water sorption to achieve the desirable water content and water state; (3) compared with permeability, the dynamic selectivity reaches the maximum value a little earlier, which may be ascribed to the faster balance of the ion hydration process compared to that of the membrane swelling process. By comparison, such a build-up of performance is not observed when the feed gas is not humidified, demonstrating that the build up of performance is mainly caused by water. To further exclude the possible metal ion–CO_2 effect (*e.g.* saturation of the cationic sites with HCO_3^- or CO_2), Pebax–$CaCl_2$ (1 : 30) after the 48 h gas permeation test is dissolved by the mixed solvent of ethanol and water. The membrane can be completely dissolved with no precipitation, which indicates that there is little $CaCO_3$ formed within membrane.

Since the residual ethanol in the membrane can coordinate with $CaCl_2$, proper annealing conditions are necessary to ensure reproductivity. The vacuum annealing temperature is set at 45 °C because higher annealing temperature may cause irreversible membrane solidification (the PA6 crystalline of Pebax is not hydrophilic enough to be swollen by water), which is unfavourable for membrane permeability. Actually, the annealing process at relatively low temperature ensures that the annealed membrane is easy to be swollen by water. The effect of annealing time is shown in Fig. 7. For Pebax, CO_2 permeability increases with annealing time, but CO_2/CH_4 and CO_2/N_2 selectivities remain at a moderate level. Interestingly, CO_2/CH_4 selectivity and CO_2/N_2 selectivity also increase with annealing time for Pebax–$CaCl_2$ (1 : 30). These facts can be explained by the effect of residual ethanol within membrane. The evidence of ethanol–$CaCl_2$ complex can be found in the FT-IR spectra (shown in Fig. S5†). The large amount of ethanol surrounding Ca^{2+} may thwart the facilitated transport of CO_2 and the salting-out effect against CH_4 and N_2, because ethanol cannot play the role of water in ion hydration and CO_2 hydration. Therefore a complete annealing process is necessary to take full advantage of the Pebax–$CaCl_2$ membrane.

The effect of operating pressure on gas separation performance is plotted in Fig. 8. Both CO_2 permeability and CO_2/CH_4 selectivity decreases with the increase of feed pressure, which is a typical indicator of the occurrence of facilitated transport.[31,42,43] However, due to the absence of fixed carriers (*e.g.* amino group) that can promote CO_2 enrichment and catalyse CO_2 hydration, the decline tendency is not so sharp as the amino-containing facilitated membranes. That is, the membranes

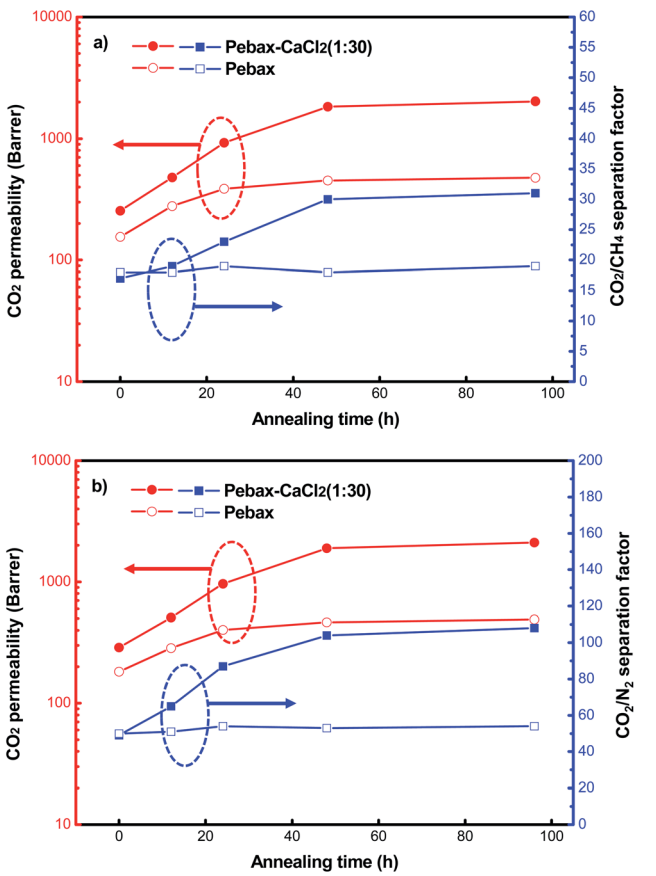

Fig. 7 Effect of annealing conditions on CO_2 capture properties of Pebax and Pebax–$CaCl_2$ (1 : 30): (a) CO_2/CH_4 separation; (b) CO_2/N_2 separation (feed gas: binary 30vol%CO_2–70vol%CH_4 gas and 10vol%CO_2–90vol%N_2, both are saturated with water vapor; temperature: 25 °C; pressure: 2 bar).

prepared in this study are less dependent on the facilitated transport mechanism, and therefore CO_2 permeability remains rather high within the whole pressure range of 1–12 bars. The pressure-dependent CO_2 capture properties in this study might be applicable for other polymer electrolyte membranes.

Operating temperature is also a crucial parameter that determines the availability of membrane. As shown in Fig. 9, CO_2 permeability gradually increases with temperature, while CO_2/gas selectivity decreases with temperature, which is attributed to the increase of gas diffusivity and polymer chain flexibility. Nevertheless, the mixed-gas CO_2/N_2 separation factor remains as high as 80 at 65 °C and 59 at 85 °C, which are significantly higher than that of pristine Pebax (20.8) under the same conditions. Considering the high CO_2 permeability up to 6000 Barrer at 85 °C, the membrane prepared in this work will be technologically attractive if the corresponding thin-film composite membranes could be successfully fabricated.

3.4 Comparison with other types of membranes

Six typical types of CO_2 separation membranes are summarized in Table 4: polyimide membranes, polyethylene oxide-based membranes, microporous organic polymer membranes, polymer-based hybrid membranes, facilitated transport membranes, and polymer electrolyte membranes. The first four types of membranes

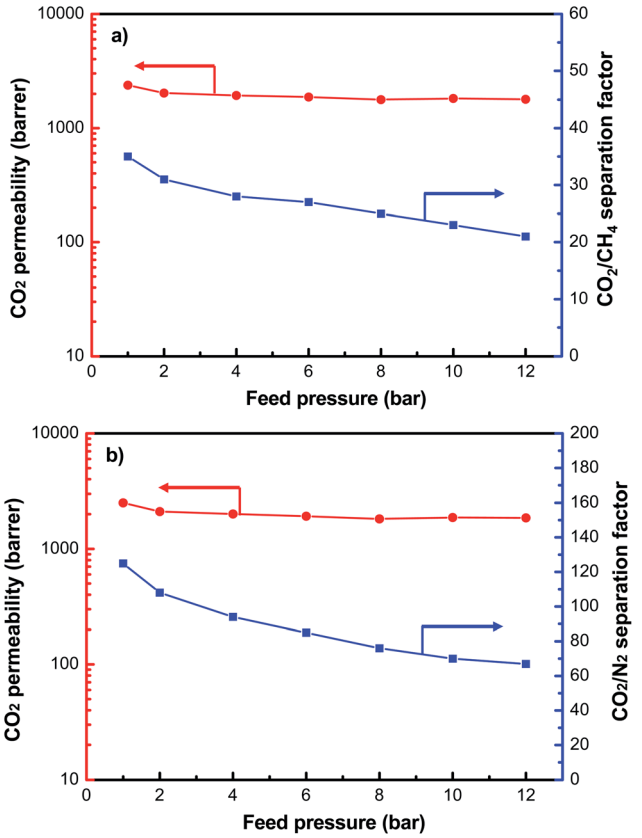

Fig. 8 Effect of feed gas pressure on CO_2 capture properties of Pebax–$CaCl_2$ (1 : 30): (a) CO_2/CH_4 separation; (b) CO_2/N_2 separation (feed gas: binary 30vol%CO_2–70vol%CH_4 gas and 10vol%CO_2–90vol% N_2, both are saturated with water vapor; temperature: 25 °C).

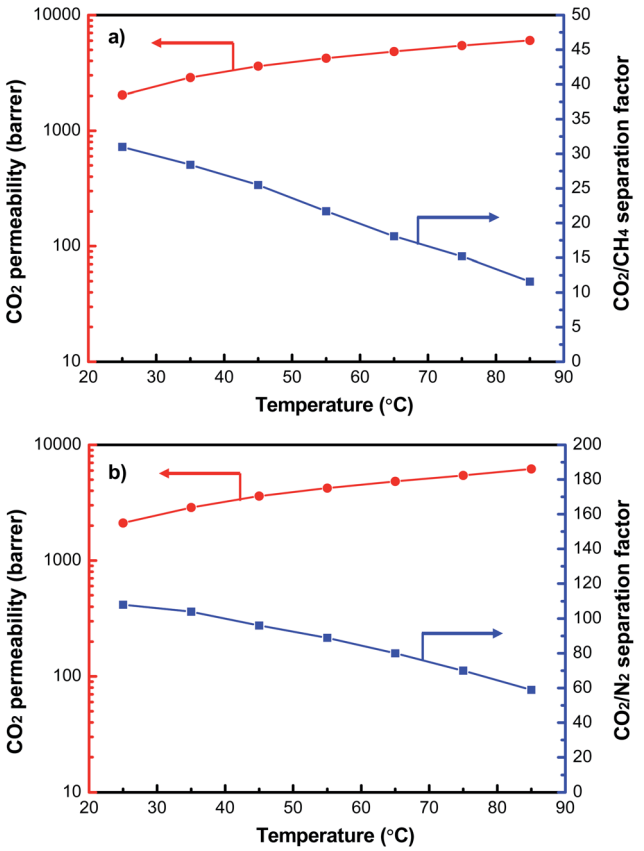

Fig. 9 Effect of operating temperature on CO_2 capture properties of Pebax–$CaCl_2$ (1 : 30): (a) CO_2/CH_4 separation; (b) CO_2/N_2 separation (feed gas: binary 30vol%CO_2–70vol%CH_4 gas and 10vol%CO_2–90vol% N_2, both are saturated with water vapor; pressure: 2 bar).

are usually operated under dry conditions, and have displayed encouraging CO_2 separation performance. Although humidification was reported to enhance CO_2 permeability, the low hydrophilicity of these membrane materials may limit their water content and therefore restrict the permeability profit under wet conditions. Besides, the selectivity mechanism of these membranes is known as the solution–diffusion mechanism, which may be essential but not sufficient to guarantee high separation factor. By comparison, facilitated transport membranes and polymer electrolyte membranes allow much higher selectivity due to the contribution from the reactivity selectivity mechanism[4] or the salting-out mechanism. Simultaneously, these membrane materials are usually hydrophilic, and therefore the water-induced swelling guarantees high CO_2 permeability under wet conditions. By further comparing facilitated transport membrane and polymer electrolyte membrane, three major advantages could be summarized for the latter: (1) facilitated transport membrane suffers more from the rapid decline of permeability with increment of operating pressure, caused by the saturation of facilitated transport carriers. (2) Facilitated transport membranes are often rich in amino groups, which may be oxidized by O_2 or SO_2 in flue gas and loose the function as facilitated transport carriers. This problem should be carefully considered before commercial application.[31,32] (3) The last but not the least important point is the low

Table 4 Comparison of membrane separation properties of other types of membranes with current work

Membrane types / Materials	CO_2 permeability (Barrer)[a]	CO_2/CH_4 selectivity[a]	CO_2/N_2 selectivity[a]	Testing conditions	Ref.
Polyimide membranes					
6FDA-durene	600[b]	15[b]	12[b]	35 °C, 10 atm, dry membrane	45
6FDA-DAM[b]	390	18[b] (24)	14	25 °C, 2 atm, dry membrane	46
Polyethylene oxide-based membranes					
Pebax® + PEGDME	606	Not reported	43	30 °C, 0.3 bar, dry membrane	47
Polyactive® + PEGDBE	750	11	40	25 °C, 10 bar, dry membrane	48
Microporous organic polymer membranes					
TR-polymers	1610	Not reported	43[b]	35 °C, 10 atm, dry membrane	13
TZPIM	2000[b]	17[b] (18[b])	26[b] (37[b])	25 °C, 3.4 bar, dry membrane	17
PIM-EA-TB	7140	10.2	13.6	25 °C, 1 bar, dry membrane	18
Polymer-based hybrid membranes					
6FDA-DAM + ZIF90A	720	27[b] (37)	22	25 °C, 2 atm, dry membrane	46
PIM-1 + organic cage	5430	11	20	25 °C, 1 atm, dry membrane	49
Facilitated transport membranes					
Poly-*N*-isopropylallylamine	(312)	Not reported	(336)	110 °C, 2 atm, humidified membrane	20
Guanidine-modified polyaniline	(3460)	(540)	Not reported	R.T., $\Delta p_i = 8.29$ kPa, humidified membrane	50
Polymer electrolyte membranes					
Pebax + $CaCl_2$	2133(2030)	38(31)	142(108)	25 °C, 3 bar, humidified membrane	This work
Pebax + $MgCl_2$	1412	42	168	25 °C, 3 bar, humidified membrane	This work
Pebax + $CaCl_2$	(6100)	(12)	(59)	85 °C, 3 bar, humidified membrane	This work

[a] The values in the bracket are for mixed-gas selectivity or separation factor. [b] Values are approximated from plots.

cost and facile fabrication of the polymer electrolyte membranes reported in this study. Theoretically, a cost-effective hydrophilic polymer is suitable as the polymer matrix, no matter whether it is capable of facilitating the transport of CO_2. Therefore, polymer electrolyte membrane as a type of high-performance, low-cost membrane is expected to find promising application in CO_2 capture. Two problems of the membranes in this study are expected to be well addressed: (1) Pebax cannot be directly fabricated into asymmetric membranes with dense skin layer, while it is quite simple to fabricate the thin-film composite membrane (including hollow fiber membrane) with Pebax as the active layer,[36,37,44] which is beneficial to enabling large-scale fabrication of the membranes in this work; (2) the selectivity of the polymer electrolyte membrane in this study cannot rival some reported facilitated transport membrane, while it can be further improved by selecting a more CO_2-selective polymer matrix (*e.g.* polyvinylamine[23] and polyallylamine[20]) or substituting chloride salts with fluoride salts or oxysalts, of which the benefits have been discussed in the recent literature.[27]

4. Conclusions

In this study, the PEO-based polymer electrolyte membrane was firstly utilized for CO_2 capture. The hydroscopic nature of salt-doped membranes endowed high amount of total water and bound water, leading to high CO_2 permeability and CO_2/gas selectivity, respectively, and most of the separation performance data are beyond the upper bounds. The content of bound water largely depended on the free hydration energy of the metal ion, and hence membranes doped with alkaline-earth metal salt outperformed those doped with alkali metal salt. The content of total water was determined by the degree of metal–polymer complexation, which should not only weaken the interactions of polar groups on polymer chains but also avoid excessive ionic-cross-linking. The findings of this study are important for the design of high-performance gas separation membranes using cost-effective materials. More polymer electrolyte membranes comprising of different types of polymers and salts are expected to be explored.

Acknowledgements

This study was financially supported by the National High Technology Research and Development Program of China (2012AA03A611), National Science Fund for Distinguished Young Scholars (21125627), Tianjin Natural Science Foundation (no. 10JCZDJC22600), and the Program of Introducing Talents of Discipline to Universities (no. B06006).

References

1 N. MacDowell, N. Florin, A. Buchard, J. Hallett, A. Galindo, G. Jackson, C. S. Adjiman, C. K. Williams, N. Shah and P. Fennell, *Energy Environ. Sci.*, 2010, **3**, 1645–1669.
2 K. Sumida, D. L. Rogow, J. A. Mason, T. M. McDonald, E. D. Bloch, Z. R. Herm, T.-H. Bae and J. R. Long, *Chem. Rev.*, 2012, **112**, 724–781.

3 D. M. D'Alessandro, B. Smit and J. R. Long, *Angew. Chem., Int. Ed.*, 2010, **49**, 6058–6082.
4 S. Li, Z. Wang, X. Yu, J. Wang and S. Wang, *Adv. Mater.*, 2012, **24**, 3196–3200.
5 Y. Yampolskii, *Macromolecules*, 2012, **45**, 3298–3311.
6 L. M. Robeson, *J. Membr. Sci.*, 1991, **62**, 165–185.
7 L. M. Robeson, *J. Membr. Sci.*, 2008, **320**, 390–400.
8 B. D. Freeman, *Macromolecules*, 1999, **32**, 375–380.
9 H. Q. Lin and B. D. Freeman, *J. Mol. Struct.*, 2005, **739**, 57–74.
10 N. B. McKeown, P. M. Budd, K. J. Msayib, B. S. Ghanem, H. J. Kingston, C. E. Tattershall, S. Makhseed, K. J. Reynolds and D. Fritsch, *Chem. – Eur. J.*, 2005, **11**, 2610–2620.
11 Y. C. Xiao, B. T. Low, S. S. Hosseini, T. S. Chung and D. R. Paul, *Prog. Polym. Sci.*, 2009, **34**, 561–580.
12 Y. C. Xiao and T. S. Chung, *Energy Environ. Sci.*, 2011, **4**, 201–208.
13 H. B. Park, C. H. Jung, Y. M. Lee, A. J. Hill, S. J. Pas, S. T. Mudie, E. Van Wagner, B. D. Freeman and D. J. Cookson, *Science*, 2007, **318**, 254–258.
14 S. H. Han, H. J. Kwon, K. Y. Kim, J. G. Seong, C. H. Park, S. Kim, C. M. Doherty, A. W. Thornton, A. J. Hill, Á. E. Lozano, K. A. Berchtold and Y. M. Lee, *Phys. Chem. Chem. Phys.*, 2012, **14**, 4365–4373.
15 F. Y. Li, Y. Xiao, T.-S. Chung and S. Kawi, *Macromolecules*, 2012, **45**, 1427–1437.
16 B. S. Ghanem, N. B. McKeown, P. M. Budd, J. D. Selbie and D. Fritsch, *Adv. Mater.*, 2008, **20**, 2766–2771.
17 N. Du, H. B. Park, G. P. Robertson, M. M. Dal-Cin, T. Visser, L. Scoles and M. D. Guiver, *Nat. Mater.*, 2011, **10**, 372–375.
18 M. Carta, R. Malpass-Evans, M. Croad, Y. Rogan, J. C. Jansen, P. Bernardo, F. Bazzarelli and N. B. McKeown, *Science*, 2013, **339**, 303–307.
19 J. Huang, J. Zou and W. S. W. Ho, *Ind. Eng. Chem. Res.*, 2008, **47**, 1261–1267.
20 Y. Zhao and W. S. Winston Ho, *J. Membr. Sci.*, 2012, **415–416**, 132–138.
21 L. A. El-Azzami and E. A. Grulke, *Ind. Eng. Chem. Res.*, 2008, **48**, 894–902.
22 L. A. El-Azzami and E. A. Grulke, *J. Membr. Sci.*, 2009, **328**, 15–22.
23 Z. Qiao, Z. Wang, C. Zhang, S. Yuan, Y. Zhu, J. Wang and S. Wang, *AIChE J.*, 2013, **59**, 215–228.
24 J. R. Du, L. Liu, A. Chakma and X. Feng, *Chem. Eng. J.*, 2010, **156**, 33–39.
25 S. R. Reijerkerk, R. Jordana, K. Nijmeijer and M. Wessling, *Int. J. Greenhouse Gas Control*, 2011, **5**, 26–36.
26 G. Q. Chen, C. A. Scholes, C. M. Doherty, A. J. Hill, G. G. Qiao and S. E. Kentish, *J. Membr. Sci.*, 2012, **409–410**, 96–104.
27 L. Zhang and R. Wang, *RSC Adv.*, 2012, **2**, 9551–9554.
28 K. Yao, Z. Wang, J. Wang and S. Wang, *Chem. Commun.*, 2012, **48**, 1766–1768.
29 S. Li, Z. Wang, C. Zhang, M. Wang, F. Yuan, J. Wang and S. Wang, *J. Membr. Sci.*, 2013, **436**, 121–131.
30 S. Zhao, Z. Wang, Z. Qiao, X. Wei, C. Zhang, J. Wang and S. Wang, *J. Mater. Chem. A*, 2013, **1**, 246–249.
31 M. Wang, Z. Wang, S. Li, C. Zhang, J. Wang and S. Wang, *Energy Environ. Sci.*, 2013, **6**, 539–551.
32 M. Wang, Z. Wang, J. Wang, Y. Zhu and S. Wang, *Energy Environ. Sci.*, 2011, **4**, 3955–3959.
33 L. Liu, A. Chakma and X. Feng, *J. Membr. Sci.*, 2008, **310**, 66–75.
34 M. Rikukawa and K. Sanui, *Prog. Polym. Sci.*, 2000, **25**, 1463–1502.
35 E. Quartarone, P. Mustarelli and A. Magistris, *Solid State Ionics*, 1998, **110**, 1–14.
36 A. Car, C. Stropnik, W. Yave and K. V. Peinemann, *Sep. Purif. Technol.*, 2008, **62**, 110–117.
37 Y. Li, S. Wang, H. Wu, J. Wang and Z. Jiang, *J. Mater. Chem.*, 2012, **22**, 19617–19620.
38 R. S. Murali, S. Sridhar, T. Sankarshana and Y. V. L. Ravikumar, *Ind. Eng. Chem. Res.*, 2010, **49**, 6530–6538.
39 W. Yave, A. Car, K. V. Peinemann, M. Q. Shaikh, K. Ratzke and F. Faupel, *J. Membr. Sci.*, 2009, **339**, 177–183.
40 J. Aaqvist, *J. Phys. Chem.*, 1990, **94**, 8021–8024.
41 R. Tahara, T. Morozumi, H. Nakamura and M. Shimomura, *J. Phys. Chem. B*, 1997, **101**, 7736–7743.
42 J. Zou and W. S. W. Ho, *J. Membr. Sci.*, 2006, **286**, 310–321.
43 L. Y. Deng, T. J. Kim and M. B. Hagg, *J. Membr. Sci.*, 2009, **340**, 154–163.
44 L. Liu, A. Chakma and X. S. Feng, *Ind. Eng. Chem. Res.*, 2005, **44**, 6874–6882.
45 L. Shao, T.-S. Chung, S. H. Goh and K. P. Pramoda, *J. Membr. Sci.*, 2005, **256**, 46–56.
46 T. H. Bae, J. S. Lee, W. L. Qiu, W. J. Koros, C. W. Jones and S. Nair, *Angew. Chem., Int. Ed.*, 2010, **49**, 9863–9866.
47 W. Yave, A. Car and K. V. Peinemann, *J. Membr. Sci.*, 2010, **350**, 124–129.
48 W. Yave, A. Car, S. S. Funari, S. P. Nunes and K. V. Peinemann, *Macromolecules*, 2010, **43**, 326–333.
49 A. F. Bushell, P. M. Budd, M. P. Attfield, J. T. A. Jones, T. Hasell, A. I. Cooper, P. Bernardo, F. Bazzarelli, G. Clarizia and J. C. Jansen, *Angew. Chem., Int. Ed.*, 2013, **52**, 1253–1256.
50 N. V. Blinova and F. Svec, *J. Membr. Sci.*, 2012, **423–424**, 514–521.